Heat Transfer Analysis of Fiberglass Insulations With and Without Foil Radiant Barriers

J.W. Rish III* and J.A. Roux†
University of Mississippi, University, Mississippi

This work compares analytical results with experimental data for the total heat transfer through typical fiberglass insulations subjected to a time-varying incident radiative heat flux and with time-varying temperature boundaries. The insulation configurations and thermal environments analyzed are consistent with conditions that exist in residential attics during the summer months. A heat transfer analysis was performed, which treats the problem as one of coupled transient conduction and radiative heat transfer in a fully participating medium (absorbing, emitting, and scattering). Computations were performed for both isotropic and anisotropic phase functions and for both gray and nongray radiative transport. Temperature data recorded for summer-time conditions in FL and MS were used to describe the boundary conditions for the heat transfer analysis. The effect of foil radiant barriers on the overall heat transfer through the insulation also was studied. Calculations are presented that compare the foil radiant barrier and no-foil cases; the foil barrier is shown to reduce the total heat transfer by about 42%. All computations used the discrete ordinates solution method to solve the radiative transport equation and a control-volume based finite difference technique to solve the energy equation.

Introduction

NUMEROUS works have been performed in order to determine the importance of various combined modes of heat transfer in fibrous insulating materials. Several different approaches have been used to attack this problem with limited success.[1-8] However, it is well known that the two dominant modes of heat transfer for fibrous insulations are radiation and gas conduction. Radiative transfer is known to be responsible for 30 to 50% of the total heat transfer in low-density fibrous insulations. Intra-fiber conduction and other mechanisms, such as convection, also occur within the medium, but for insulations such as fiberglass, these effects have been shown to be negligible at moderate temperatures.[9]

The use of reflective radiant barriers (aluminum foil) in conjunction with standard fibrous insulation configurations is presently being investigated as a means of improving the energy efficiency of residential dwellings. Radiant barriers provide a means of reducing the total heat transfer through fibrous insulations by either blocking most of the incident radiation or by acting to reduce the emissivity of high-temperature surfaces, which are sources of the incident radiation. Experimental measurements by Fairey[10] indicate that radiant barriers may reduce the total heat transfer through attic insulations during the summer months by as much as 42%.

Experimental work such as Fairey's is both costly and time consuming. A suitable analytical model would reduce the amount of experimental effort required to evaluate the influence of radiant barriers on the heat transfer through fibrous insulations and provide an enhanced understanding of the experimental results. An efficient and accurate analytical model that is applicable to this problem has been developed.[11] Nevertheless, analytical studies concerning radiative transport phenomena in participating media are often impeded by the limited availability of radiative properties (spectral absorption and scattering coefficients) for the materials under consideration. In conjunction with this present work, the spectral radiative properties of fiberglass were determined in a concurrent study from experimental spectral directional-hemispherical reflectance data.[12]

The purpose of this paper is to present heat-transfer results for non-steady-state conditions in a standard 6-in (R-19) fiberglass batt. Results are shown for three sets of temperature boundary conditions involving measured surface temperatures that are typical for insulations in summer-time attic environments. These boundary conditions correspond to the following attic insulation configurations: fiberglass insulation with no foil radiant barrier; the use of a foil radiant barrier on the rafters; and the placement of a foil radiant barrier on the top surface of the insulation. Comparisons are made with experimental heat transfer measurements reported by Fairey[10] in order to validate the analytical model. The results are extended to include theoretical heat transfer computations based upon experimental temperature data acquired in MS.[11] The analytical approach consists of a control volume based finite difference scheme[13] for solving the energy equation simultaneously with the one-dimensional radiative transport equation. An iterative solution procedure was used in which the radiative transport equation was solved employing the approach presented by Chandrasekhar.[14] The analysis indicates that in cases where foil radiation barriers are used, the net heat transfer through the insulation is significantly reduced.

Problem Statement

The basic geometry for the heat transfer analysis is shown in Fig. 1. The physical configuration consists of a fiberglass insulation layer of thickness H which is bounded on the lower surface (surface 1) by an opaque substrate (gypsum board) and on the upper surface (surface 2) by either a layer of air or a reflective radiant barrier. A third surface (surface 3) located above the insulation layer is assumed to emit radiation at some characteristic temperature T_r, and the energy radiated from surface 3 (roof) is assumed to be diffusely incident upon the insulation layer. The temperatures, reflectances, and emissivities of each surface are assumed to be known.

The fiberglass is treated as a layer of air that contains a matrix of glass fibers, i.e., air acts as a host medium to the fiber array. Therefore, the refractive index of the top insulation interface should be the same as that of air which is unity.

Received Jan. 10, 1986; revision received April 1, 1986; presented as Paper 86-1294 at the AIAA/ASME 4th Thermophysics and Heat Transfer Conference, Boston, MA, June 2-4, 1986.

*Research Assistant; presently Mechanical Engineer, Naval Coastal Systems Center, Panama City, FL. Member AIAA.

†Associate Professor, Department of Mechanical Engineering. Member AIAA.

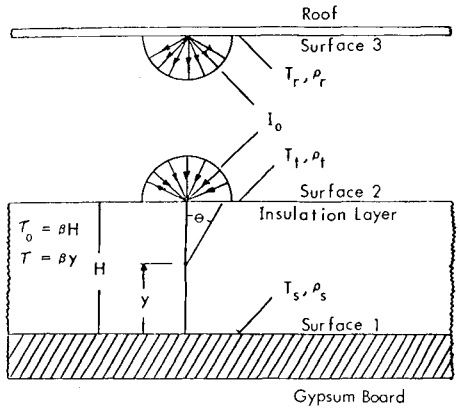

Fig. 1 Geometry and coordinate system.

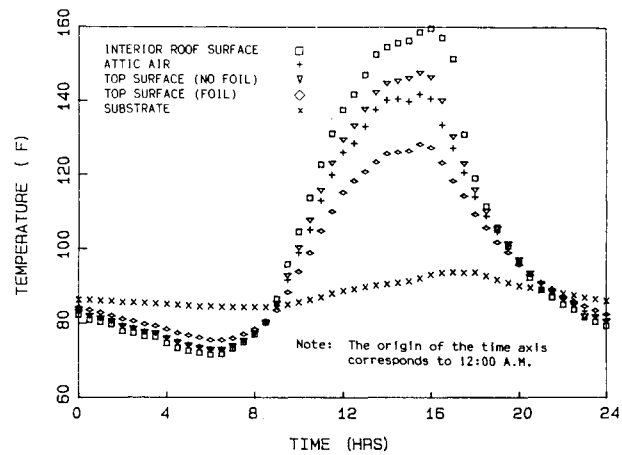

Fig. 2 Attic surface temperature-time histories for foil and no foil insulations. The temperature data were taken in a North Mississippi residence on June 2, 1985.

Heat transfer through this composite medium is assumed to be one-dimensional, axisymmetric, coupled conduction and radiation. The insulation layer is assumed to absorb, emit, and scatter radiation. Although scattering within the medium is known to be anisotropic, both isotropic and anisotropic scattering phase functions are considered. Other assumptions with regard to transport properties are: the specific heat is considered to be constant, but the thermal conductivity is taken to be a function of temperature; and the radiative properties of the insulation layer are assumed to be constant throughout the medium and independent of temperature.

Two distinct heat transfer problems are formulated for the geometry of Fig. 1. The first problem is the determination of the heat transfer to the substrate through an unshielded insulation (no-foil) for which the boundary temperatures T_s, T_t, and T_r are known for surfaces 1, 2, and 3 respectively. An analogous problem also is considered in which a foil radiant barrier is attached to the rafters. These two situations are distinguished from each other by assigning different emissivities (or reflectances) to surface 3. Thermal radiation from surface 3, which has an emissivity ε_r, is assumed to be diffusely incident upon surface 2 which has a reflectance ρ_t equal to zero. The second problem is to determine the effect on the total heat transfer that would result from placing a foil radiation barrier immediately adjacent to surface 2 (foil on top).

The two heat transfer situations just described are used to model the heat transport phenomena which occurs in a typical attic environment. Surface 1 represents the gypsum board, surface 2 represents the top surface of the insulation layer, and surface 3 represents the interior surface of a roof. Boundary conditions used to obtain the theoretical results are based upon experimentally measured temperature-time histories[10,11] for the top surface of the gypsum board, the top surface of the insulation, and the interior roof surface (surfaces 1, 2, and 3 respectively). Temperature data were obtained by instrumenting an attic with thermocouples and recording the surface temperatures at regular intervals. Temperature-time histories for two different insulation configurations on a typical summer day in MS are shown in Fig. 2.

Analysis

The governing equations for the heat transfer analysis are the one-dimensional axisymmetric integro-differential equation of radiative transfer and the one-dimensional energy equation. The determination of the net heat transfer at any point within the medium is an iterative process because of the inherent coupling that exists between these two equations. The solution process involves three major steps: a temperature profile across the medium must be assumed; the radiative transport equation is then solved for a local radiative heat flux; and the energy equation is solved in an iterative fashion using a control-volume based finite difference scheme in order to converge on a temperature field.

Solution of the Transport Equation

The one-dimensional radiative transport equation in a plane parallel medium which absorbs, emits, and anisotropically scatters is given by[15]

$$\frac{dI(\tau,\mu)}{d\tau} = -\frac{I(\tau,\mu)}{\mu} + \frac{W}{2\mu}\int_{-1}^{1} I(\tau,\mu')\Phi(\mu,\mu')\,d\mu' + \frac{(1-W)n^2 I_b(\tau)}{\mu} \tag{1}$$

Here τ is the optical depth, μ is the cosine of the polar angle θ, W is the albedo of scattering, $I(\tau,\mu)$ is the radiative intensity at depth τ and in the direction given by μ, n is the refractive index, $I_b(\tau)$ is Planck's blackbody intensity function, and $\Phi(\mu,\mu')$ is the scattering phase function. The phase function can be represented by an N-term series of Legendre polynomials as

$$\Phi(\mu,\mu') = \sum_{\ell=0}^{N} A_\ell P_\ell(\mu) P_\ell(\mu') \tag{2}$$

where the coefficients, A_ℓ, can be determined either analytically or through the use of experimental data. For isotropic scattering, the phase function takes on a value of unity.

A semi-analytical solution to Eq. (1) is achieved by using the method of discrete ordinates.[11,16-18] The solution is achieved by replacing the integral term in Eq. (1) with an m-order Gaussian quadrature to yield the discrete ordinate approximation of the radiative transport equation,

$$\frac{dI(\tau,\mu_i)}{d\tau} = -\frac{I(\tau,\mu_i)}{\mu_i} + \frac{W}{2\mu_i}\sum_{j=1}^{m} a_j I(\tau,\mu_j)\sum_{\ell=0}^{N} A_\ell P_\ell(\mu_i) P_\ell(\mu_j) + \frac{(1-W)n^2 I_b(\tau)}{\mu_i}, \qquad i = 1,\ldots,m \tag{3}$$

The μ_i's and μ_j's in this expression are the quadrature points, and the a_j's are the quadrature weights. Equation (3) represents a system of first-order, linear, inhomogeneous, ordinary differential equations, which may be solved analytically by using classical methods for systems of equations. The set of

general solutions to Eq. (3) is given by[18]

$$I(\tau,\mu_i)=\sum_{j=1}^{m/2}(1-\lambda_j\mu_j)\times\left\{\frac{C_j e^{\lambda_j\tau}Y(\mu_i,\lambda_j)}{1+\mu_i\lambda_j}+\frac{C_{m+1-j}e^{-\lambda_j\tau}Y(\mu_i,-\lambda_j)}{1-\mu_i\lambda_j}\right\}+(1-W)n^2\sum_{j=1}^{m/2}\frac{K_{m+1-j}Y(\mu_i,-\lambda_j)}{1-\mu_i\lambda_j}\int_0^{\tau}I_b(t)\,e^{-\lambda_j(\tau-t)}\,dt-(1-W)n^2\sum_{j=1}^{m/2}\frac{K_jY(\mu_i,\lambda_j)}{1+\mu_i\lambda_j}\int_{\tau}^{\tau_0}I_b(t)\,e^{-\lambda_j(t-\tau)}\,dt \qquad i=1,\ldots,m \quad (4)$$

where τ_0 is the optical thickness of the medium, the C_j's are the m constants of integration which must satisfy a given set of boundary conditions. The λ_j's are the $m/2$ positive eigen values for the system of equations described by Eq. (3), and which must satisfy the following relationship

$$\sum_{k=1}^{m}\frac{a_k}{1+\mu_k\lambda_j}Y(\mu_k,\lambda_j)=\frac{2}{W} \quad (5)$$

The Y-functions correspond to anisotropic scattering effects throughout the medium. They are defined by

$$Y(\mu_i,\pm\lambda_j)=\sum_{\ell=0}^{N}A_\ell P_\ell(\mu_i)\xi_\ell(\pm\lambda_j) \qquad i=1,\ldots,m; \qquad j=1,\ldots,m/2 \quad (6)$$

subject to the restriction that $2m-1>2N$, and where the ξ_ℓ's are determined from the recursion formula

$$\xi_0=1; \qquad \xi_1(\lambda_j)=\frac{(WA_0-1)}{\lambda_j} \quad (7a)$$

$$\xi_{\ell+1}(\lambda_j)=\xi_\ell(\lambda_j)\frac{WA_\ell-(2\ell+1)}{\lambda_j(\ell+1)}-\frac{\ell\xi_{\ell-1}(\lambda_j)}{\ell+1} \qquad \ell=1,\ldots,N-1 \quad (7b)$$

The K_j's are a set of constants associated with the particular solutions to Eq. (2) which must satisfy the system of equations given by

$$\sum_{j=1}^{m/2}K_j\left\{\frac{Y(\mu_i,\lambda_j)}{1+\mu_i\lambda_j}-\frac{Y(\mu_i,-\lambda_j)}{1-\mu_i\lambda_j}\right\}=\frac{1}{\mu_i} \qquad i=1,\ldots,m/2 \quad (8)$$

$$K_{m+1-j}=-K_j, \qquad j=1,\ldots,m/2 \quad (9)$$

The C_j's are evaluated by applying the radiative boundary conditions given by

$$I(0,\mu_i)=(1-\rho_s)I_b(T_s)+\rho_sI(0,-\mu_i), \qquad i=1,\ldots,m/2 \quad (10a)$$

and either

$$I(\tau_0,-\mu_i)=(1-\rho_t)I_b(T_t)+\rho_tI(0,-\mu_i) \qquad i=1,\ldots,m/2 \quad (10b)$$

or

$$I(\tau_0,-\mu_i)=(1-\rho_r)I_b(T_r)+\rho_rI(0,-\mu_i) \qquad i=1,\ldots,m/2 \quad (10c)$$

where ρ_s is the reflectance of the substrate, ρ_t is the reflectance of the top surface, and ρ_r is the reflectance of the roof. Substitution of Eq. (4) into Eqs. (10) yields the necessary equations to obtain the C_j values.

The net radiative heat flux at depth τ can now be obtained by integrating the intensity as follows:

$$Q_R(\tau)=2\pi\int_{-1}^{1}I(\tau,\mu)\mu\,d\mu\cong 2\pi\sum_{i=1}^{m}I(\tau,\mu_i)\mu_i a_i \quad (11)$$

Substituting Eq. (4) into Eq. (12) and simplifying yields

$$Q_R(\tau)=-\frac{4\pi(1-W)}{W}\sum_{j=1}^{m/2}\frac{(1-\lambda_j\mu_j)}{\lambda_j}\left[C_je^{\lambda_j\tau}-C_{m+1-j}e^{-\lambda_j\tau}\right]-\frac{4\pi(1-W)^2n^2}{W}\sum_{j=1}^{m/2}\frac{K_j}{\lambda_j}\left\{\int_0^{\tau}I_b(t)\,e^{-\lambda_j(\tau-t)}\,dt-\int_{\tau}^{\tau_0}I_b(t)\,e^{-\lambda_j(t-\tau)}\,dt\right\} \quad (12)$$

The two integral terms in Eq. (12) can be evaluated using a numerical technique described in Ref. 11. For the case of a nongray medium, the net radiative heat flux at depth y is given by

$$Q_R(y)=2\pi\int_0^{\infty}\int_{-1}^{1}I(y,\mu)\mu\,d\mu\,d\Lambda \quad (13)$$

where the outside integration is performed with respect to wavelength, Λ, and where τ, W, λ_j's, C_j's and K_j's are wavelength dependent quantities.

A radiative band model (picket fence model), in which the aforementioned quantities are assumed to be constants in each of a finite number of wavelength intervals, is used to perform the integration indicated in Eq. (13). This can be expressed as

$$Q_R(y)=\sum_{p=1}^{L}Q_{R_p}^{\Lambda}(y) \quad (14)$$

where $Q_{R_p}^{\Lambda}$ is the radiative flux for the pth wavelength interval and L is the total number of wavelength intervals considered.

Solution of Energy Equation

The one-dimensional energy equation for transient coupled conduction and radiation in a planar medium is given by

$$\rho C_p\frac{\partial T}{\partial t}=\frac{\partial}{\partial y}\left(k\frac{\partial T}{\partial y}\right)-\frac{\partial Q_R}{\partial y}(y,t,T) \quad (15)$$

where ρ is the density of the medium, C_p is the specific heat of the medium, and k is the thermal conductivity of the medium. The independent variables, t and y, are time and space variables respectively. For a radiatively gray medium, Eq. (15) can be transformed into optical coordinates by using the relationship $d\tau=\beta\,dy$ where β is a gray extinction coefficient. Further non-dimensionalization yields

$$N_t\frac{\partial\theta}{\partial t^*}=N_c\frac{\partial}{\partial\tau}\left(k^*\frac{\partial\theta}{\partial\tau}\right)-\theta_N^4\frac{\partial q_R}{\partial\tau} \quad (16)$$

where the dimensionless variables are defined by

$$\theta = T/T_s; \qquad \theta_N = T_N/T_s;$$

$$t^* = t/\eta; \qquad k^* = k/k_s; \qquad q_R = Q_R/\sigma T_N^4 \tag{17}$$

The quantities T_N, η, and k_s represent a constant reference temperature, a characteristic time, and the thermal conductivity of the medium evaluated at the substrate temperature respectively. The dimensionless parameters N_t and N_c are given by

$$N_t = \frac{\rho C_p}{\sigma T_s^3 \beta \eta}; \qquad N_c = \frac{k_s \beta}{\sigma T_s^3} \tag{18}$$

For the nongray media case, it is more convenient to use a dimensionless form of the energy equation in which τ is replaced by $y^* = y/H$ so that N_t and N_c become

$$N_t = \frac{H\rho C_p}{\sigma T_s^3 \eta}; \qquad N_c = \frac{k_s}{H\sigma T_s^3} \tag{19}$$

The parameter N_t can be interpreted as the ratio of the heat capacity of the medium to the heat radiated at the substrate, and N_c, which is similar in form to the conduction to radiation parameter defined by Viskanta,[19] represents the ratio of conduction to radiation at the substrate.

The boundary conditions applicable to this problem for the gray media case are

$$\theta(0, t^*) = 1 \tag{20a}$$

$$\theta(\tau_0, t^*) = T_t(t^*)/T_s(t^*) \tag{20b}$$

subject to the initial conditions

$$\theta(\tau, 0) = f_0(\tau) \tag{20c}$$

where f_0 represents a guessed temperature distribution at time $t^* = 0$. For purposes of this study, f_0 is given by

$$f_0(\tau) = \{[\theta(\tau_0, 0) - 1]/\tau_0\}\tau + 1 \tag{21}$$

The use of temperature boundary conditions as opposed to flux boundary conditions is dictated by two factors: temperature data may be obtained with very simple instrumentation and the effects of surface convection are implicitly contained in the temperature data.

The fiberglass thermal conductivity is based upon a relationship proposed by Houston[4] which is given by

$$k = k_{\text{air}} + 0.0095\rho \tag{22}$$

where k_{air} is assumed to be a function of temperature.

Discretization of the energy equation is accomplished by using a control volume based finite difference scheme[13] with a fully implicit time discretization procedure. Temperature nodes are assumed to be located within each control volume and radiation nodes are located on the control volume boundaries. Solutions for the resulting tridiagonal system of equations were accomplished by dividing the calculation domain into 95 equal size control volumes. This yields a computational mesh, which contains a total of 97 temperature nodes and 96 radiation nodes.

Results were obtained using a 16-point single Gaussian quadrature in the radiative transport equation. The radiative boundary conditions were applied, and the coupled conduction and radiation model was solved for flux-time histories at the substrate. Convergence was assumed to occur when the spatial temperature profile throughout the insulation layer was found to have a maximum change of less than 0.06°F between successive iterations. All computations were performed on an IBM PC-XT/370 using VS FORTRAN. Execution times were typically about 7 min for each gray heat-transfer case, and about 1½ for each nongray heat-transfer case.

Results and Discussion

The heat transfer analysis was performed for both gray and nongray radiative properties and for both isotropic and anisotropic phase functions. Legendre coefficients for the anisotropic phase function were taken from a 20-term phase function expansion reported by Schuetz.[20] Only the first 10 terms of this expansion were used in the present analysis in order to be consistent with the radiative properties determined by Yeh.[12] The radiative properties used in this study are given in Tables 1 and 2. Table 1 contains the gray albedos and extinction coefficients, and Table 2 contains the albedos and extinction coefficients used in the picket fence model in Ref. 11.

Validation of the heat transfer model was accomplished by making comparisons first with steady-state guarded hot plate measurements reported by Houston,[4] then with transient heat transfer measurements published by Fairey.[10] Details for the steady-state comparisons can be found in Ref. 11, and thus will not be duplicated here. However, selected results from the comparisons with Houston's data[11] corresponding to the transport property assumptions cited earlier can be summarized as follows:

1) The maximum percentage error between the total heat transfer predictions and the experimental measurements for the case of nongray radiative transfer and isotropic scattering was 3.54%;

2) The maximum percentage error between the total heat transfer predictions and the experimental measurements for the case of nongray radiative transfer and anisotropic scattering was 2.60%;

3) The maximum percentage error for gray radiative transfer and isotropic scattering was −6.29%;

4) The maximum percentage error for gray radiative transfer and anisotropic scattering was −6.89%.

These results imply that the nongray radiative transfer model yields more accurate results than does the gray radiative transfer model; however, the gray heat transfer predictions are in very good agreement with the experimental data (errors on the order of −2.5 to −3%) for all cases within the temperature range of interest (10-160 deg Fahrenheit). Only slight differences were observed in the heat transfer predictions for isotropic and anisotropic scattering models.

Upon completing the model validation for steady-state conditions, the next step was to proceed with the time-dependent analysis appropriate for realistic thermal environments.

Table 1 Gray radiative properties

Scattering model	W	β, 1/in.
Isotropic	0.250	10.266
Anisotropic	0.465	14.755

Table 2 Radiative properties for the picket fence model

	Isotropic scattering			Anisotropic scattering ($N = 9$)		
No.	Interval, μm	β, 1/in.	W	Interval, μm	β, 1/in.	W
1	3.0- 5.0	3.556	0.620	—	9.652	0.880
2	5.0- 6.5	4.572	0.400	5-7	10.414	0.700
3	6.5- 9.0	9.144	0.160	7-9	11.938	0.380
4	9.0-13.0	11.938	0.240	—	18.034	0.510
5	13.0-16.0	10.414	0.180	—	14.986	0.440
6	16.0-20.0	9.652	0.120	—	12.446	0.330
7	20.0-35.0	11.600	0.146	—	16.764	0.378
8	35.0-60.0	9.700	0.146	—	13.970	0.378
9	60.0-80.0	8.550	0.146	—	12.192	0.378

Boundary conditions for this case (both radiative and conductive) are based upon experimentally measured temperatures such as those presented in Fig. 2. The required temperatures for the attic heat transfer analysis are the substrate temperature (surface 1), the top surface temperature (surface 2), and the roof temperature (surface 3). Reflectance also must be known for each of these respective surfaces. Since the substrate in this case is gypsum board, a reflectance of $\rho_s = 0.15$ was used. The reflectance of the roof decking was taken to be $\rho_r = 0$ in the absence of a reflective radiant barrier and $\rho_r = 0.95$ when a reflective radiant barrier was attached to the rafters. The top surface reflectance is given by $\rho_t = 0$ in the absence of a reflective radiant barrier and by $\rho_t = 0.95$ if a reflective radiant barrier is placed upon the top surface of the insulation. The location of the radiation barrier dictates whether the top surface boundary condition corresponds to Eq. (10b) or Eq. (10c).

In order to extend the validation process to attic heat transfer situations, the heat transfer model was used in conjunction with temperature-time histories measured by the Florida Solar Energy Center (FSEC)[10] in order to predict the associated substrate flux-time histories and compare these fluxes with experimental measurements. The temperature measurements were made for two different insulation configurations. In the first case, temperature data were recorded for a 24-h period in a test cell containing a standard 6-in. (R-19) fiberglass insulation, while in the second case, temperature data for the same 24-h period was obtained for another test cell, which had aluminum foil attached to the rafters. Specially calibrated heat flux meters were attached to the top surface of the gypsum board in each cell, and heat flux measurements were recorded at the same time interval as for the temperature measurements. A 15-min time interval was used in recording the data.

Theoretical heat fluxes were computed for each FSEC temperature data set using three different radiation models. These were 1) gray properties for an isotropically scattering medium; 2) gray properties for an anisotropically scattering medium; and 3) nongray properties for an anisotropically scattering medium. A 10-min time step was used in the gray calculations, and a 15-min time step was used in nongray calculations. The computer execution times required to generate each 24-h flux-time history were about 7 min for the gray cases, and from 1 to 2 h for the nongray cases.

The predicted flux-time histories for all 6 runs are presented in Fig. 3. The sign convention has been altered so that heat flow to the substrate is positive, and heat flow toward the top surface of the insulation is negative. This was done in order to allow a direct comparison with the FSEC's measured heat fluxes.

The comparisons of the different radiation models presented in Fig. 3 lead to several interesting observations: heat transfer through the insulation in the radiant barrier test cell is significantly reduced over that for the standard insulation configuration during the solar heating period of the day; heat transfer predictions for isotropic and anisotropic scattering with gray radiative properties are practically indistinguishable from one another for each respective test cell; and nongray heat transfer predictions are extremely close to the gray predictions for the radiant barrier test cell, but the corresponding curves for the standard test cell separate slightly during the peak heating period. This is primarily due to the much larger temperature gradients that exist within the insulation layer in the standard test cell and the ability of the nongray models to account for shifts that occur in the peak of the blackbody intensity curve with increasing temperature. Based upon these comparisons and the long computer run times for the nongray models, a decision was made to use the gray isotropically scattering model in all ensuing studies.

Figure 4 is a comparison of the predicted flux-time histories with the FSEC's experimental measurements for both test cells. The gray isotropically scattering model was used to generate the analytical results. The predicted curves show reasonable agreement with the experimental data, and it can be concluded that the heat transfer model is capable of providing an accurate simulation of the time-dependent attic heat transfer process. The differences between the theoretical

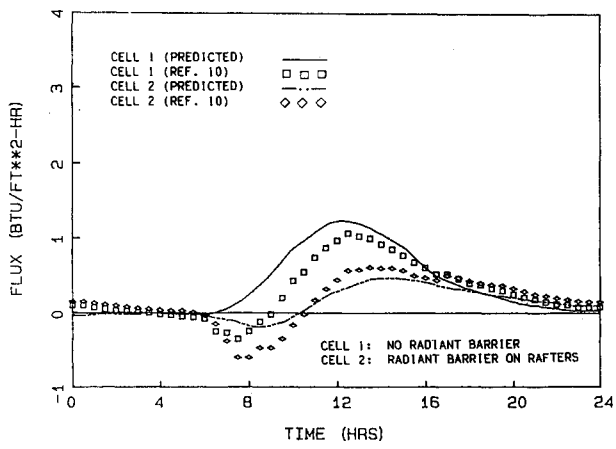

Fig. 4 Comparison of predicted substrate flux-time histories with the Florida Solar Energy Center's experimental data for June 15, 1982. Theoretical curves were determined with the gray isotropically scattering model.

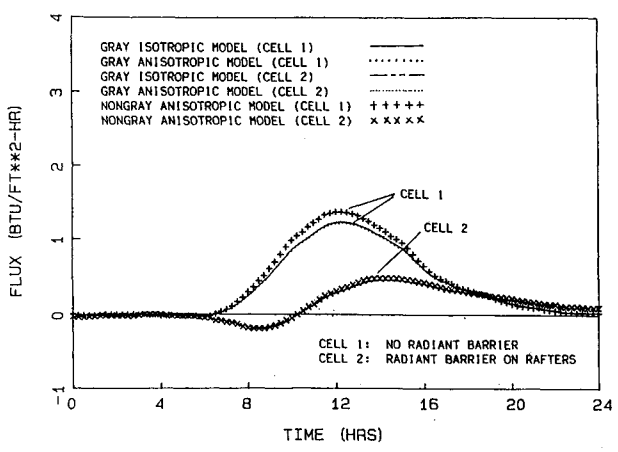

Fig. 3 Predicted flux-time histories at the substrate for June 15, 1982, based on Florida Solar Energy Center temperature data.

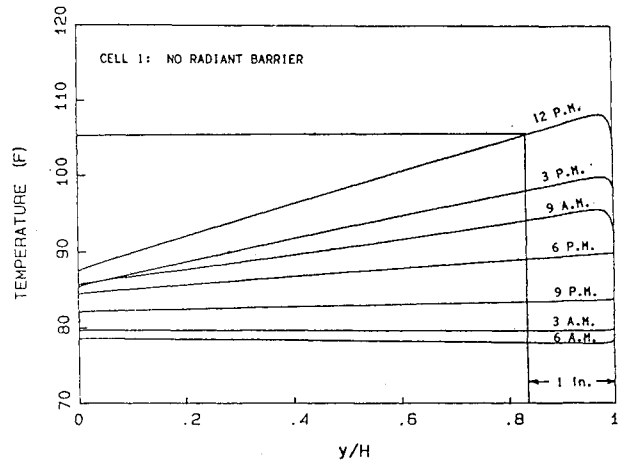

Fig. 5 Predicted spatial temperature profiles at various times of the day for the Florida Solar Energy Center's no foil test cell on June 15, 1982.

curves and the data may be due to convective currents, thermal capacitance effects from the sheetrock layer, and uncertainties in the heat flux meters.

Spatial temperature profiles were computed in addition to the substrate flux-time histories. Figure 5 is a plot of the theoretical spatial temperature profiles within the insulation layer at 3-h intervals corresponding to the FSEC's standard test cell. In the absence of a strong incident radiative flux (at night), the temperature profiles are typically quite linear. However, during the solar heating period, the temperature profiles develop an extremum near the top surface of the insulation. This peak may be attributed to the absorption and re-emission of radiation by the insulation. The temperature peak indicates that the insulation layer is actually heating the attic air. Experimental verification of this type of behavior has been made by Fairey,[10] who noted that, during the solar heating portion of the day, the temperature 1 in below the top surface of the insulation was approximately the same as the attic air temperature.

Figure 6 is a plot of the theoretical substrate flux-time histories that were computed from the temperature data presented in Fig. 2. The solid line represents the flux-time history for a standard 6-in fiberglass batt with no radiation barrier, and the dashed line is the flux-time history for an adjacent fiberglass batt, which has an aluminum foil radiation barrier placed upon its top surface. Integrating these two curves with respect to time yields the total heat load on the dwelling area (through the attic) on a per area basis for the 24-h period. A direct comparison of the integrated values indicates that the

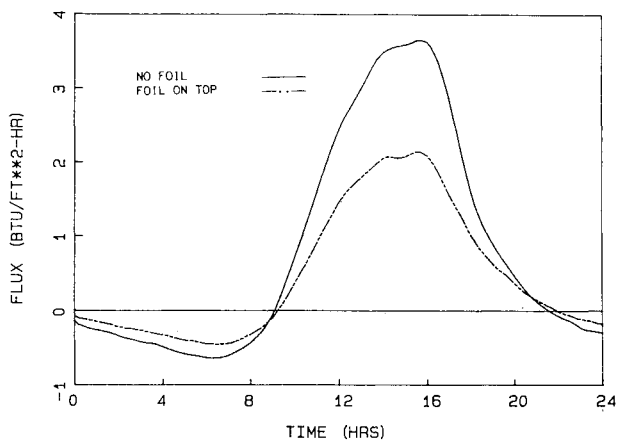

Fig. 6 Predicted substrate flux-time histories for June 2, 1985, based upon temperature data obtained in a North Mississippi residence.

Table 3 Integrated total heat fluxes over a 24-h period for selected summer days

Date	Condition	$\int Q\,dt$, Btu/ft^2	Percentage reduction
8/29/84	Unshielded	15.01	—
	Shielded	8.67	42
6/2/85	Unshielded	20.02	—
	Shielded	11.57	42
6/16/85	Unshielded	17.62	—
	Shielded	10.62	40

radiation barrier reduces the 24-h heat load by 42%. This trend is consistent throughout the summer (on clear days) as can be seen in the summary presented in Table 3. The 42% reduction also is in agreement with experimental values determined by the FSEC. A close examination of Fig. 6 shows that not only does the radiation barrier impede heat flow to the substrate during the day, but it also retards heat flow away from the substrate at night (through the insulation).

A more complete understanding of the influence of radiation on the insulation heat transfer processes for each test case can be obtained by looking at the spatial heat flux profiles presented in Figs. 7 and 8. Figure 7 is a plot of the theoretical spatial heat flux profiles through the insulation layer in the unshielded batt during the peak heating portion of the day (3:00 p.m.). In the middle of the batt, the radiation and conduction heat transfer components are very nearly the same ($Q_R/Q_{\text{total}} = 0.47$). This situation is altered considerably near the boundaries. Conduction at the substrate represents approximately 77% of the total heat transfer; but at the top boundary the influence of the large incident radiative heat flux is readily apparent. The radiative effects at the top surface are countered by convective cooling, which causes the conduction flux profile to move into the positive range. A temperature inversion should occur at the point where the conductive flux is zero. The incident radiation at the top surface is rapidly attenuated due to absorption and scattering by the insulation, and radiation effects within the insulation are largely due to emission.

Figure 8 is a plot of the theoretical spatial heat flux profiles through the insulation layer for the radiant barrier batt. The reflective surface tends to reduce radiation effects near the top boundary, but radiation effects due to emission are still strong within the insulation layer. The conductive flux component does not change signs; therefore no temperature inversion should occur within the medium.

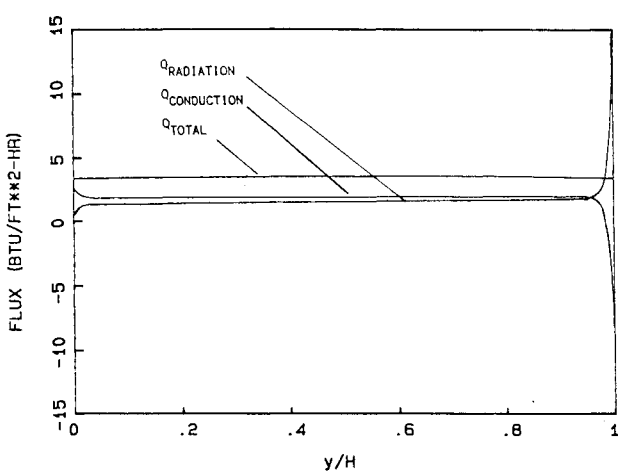

Fig. 7 Predicted spatial flux profiles for the no-foil fiberglass batt at 3:00 p.m. on June 2, 1985.

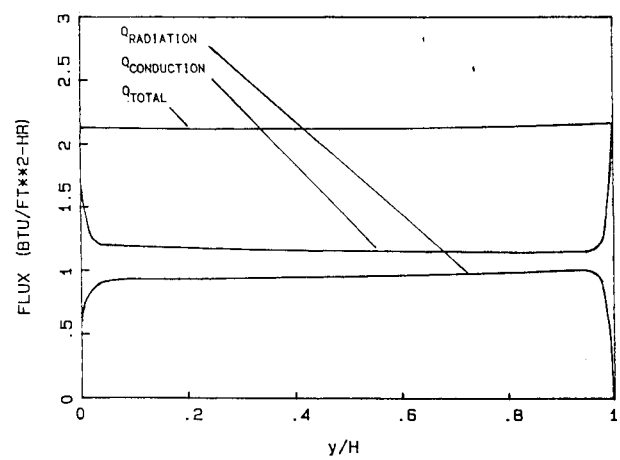

Fig. 8 Predicted spatial flux profiles in the foil fiberglass batt (foil on top) at 3:00 p.m. on June 2, 1985.

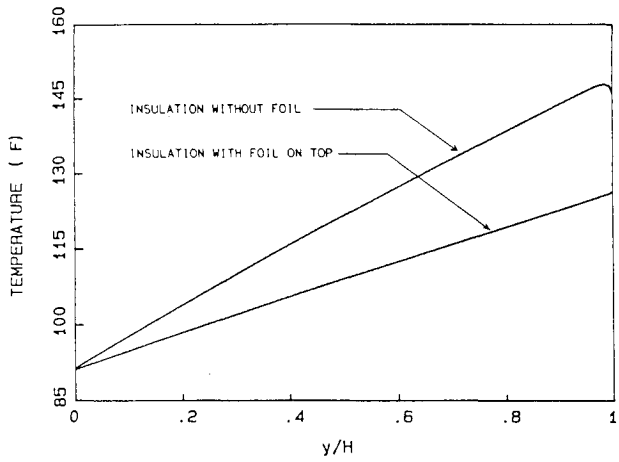

Fig. 9 Predicted spatial temperature profiles for the foil and no-foil fiberglass batts at 3:00 p.m. on June 2, 1985.

Temperature profiles corresponding to the flux profiles in Figs. 7 and 8 are presented in Fig. 9. As would be expected, a temperature inversion is present near the top surface of the unshielded insulation layer. However, no such temperature inversion is present in the shielded insulation; and the slope of the temperature profile for the shielded insulation is approximately a factor of two lower than that for the unshielded insulation, which indicates that the radiation barrier has reduced both the conductive and radiative components of the total heat transfer.

Conclusions

Theoretical heat transfer results based upon actual attic temperature data have been obtained. These results indicate that reflective radiant barriers effectively reduce the total heat transfer through the attic insulation layer to a residential dwelling space by about 42%. Spatial flux and temperature profiles that are consistent with the physical phenomena that occur in an attic thermal environment have been obtained. The flux profiles show that radiation effects account for about (interior of batt) 45 to 47% of the total heat transfer through the insulation with the exception of regions near the boundaries. This finding is consistent with the present understanding of heat transfer processes through fibrous insulations. These results show that significant energy saving can be achieved by the use of radiant foil barriers as a retrofit technique in residential attic insulation schemes.

Acknowledgment

This work was funded in part by the National Science Foundation under grant MEA-8217974.

References

[1]Verschoor, J.D. and Greebler, P., "Heat Transfer by Gas Conduction and Radiation in Fibrous Insulations," *Transactions of the ASME*, Vol. 74, 1952, pp. 961-968.

[2]Hager, N.E. Jr. and Steere, R.C., "Radiant Heat Transfer in Fibrous Thermal Insulations," *Journal of Applied Physics*, Vol. 38, Nov. 1967, pp. 4663-4668.

[3]Pelanne, C.M., "Heat Flow Principles in Thermal Insulations," *Journal of Thermal Insulation*, Vol. 1, July 1977, pp. 48-80.

[4]Houston, R.L., "Combined Radiation and Conduction in a Non-gray Participating Medium that Absorbs, Emits, and Anisotropically Scatters," Ph.D. Dissertation, The Ohio State University, OH, 1980.

[5]Houston, R.L. and Korpela, S.A., "Heat Transfer Through Fiberglass Insulations," *Proceedings of the 7th International Heat Transfer Conference*, Vol. 2, 1982, pp. 499-504.

[6]Tong, T.W. and Tien, C.L., "Radiative Heat Transfer in Fibrous Insulations—Part I: Analytical Study," *Journal of Heat Transfer*, Vol. 105, No. 1, 1983, pp. 70-75.

[7]Tong, T.W., Yang, Q.S., and Tien, C.L., "Radiative Heat Transfer in Fibrous Insulations—Part II: Experimental Study," *Journal of Heat Transfer*, Vol. 105, No. 2, 1983, pp. 76-81.

[8]Tong, T.W. and Tien, C.L., "Analytical Models for Thermal Radiation in Fibrous Insulations," *Journal of Thermal Insulation*, Vol. 4, July 1980, pp. 27-44.

[9]Tien, C.L. and Cunnington, G.R., "Cryogenic Insulation Heat Transfer," *Advanced Heat Transfer*, Vol. 9, 1973, pp. 349.

[10]Fairey, P.W., "Effects of Infrared Radiation Barriers on the Effective Thermal Resistance of Building Envelopes," *ASHRAE/DOE Conference on Thermal Performance of the Exterior Envelopes of Buildings II*, Las Vegas, NV, Dec. 1982.

[11]Rish, J.W. III, "A Numerical and Experimental Investigation of Coupled Radiative and Conductive Transient Heat Transfer in Fibrous Insulations," Ph.D. Dissertation, The University of Mississippi, University, MS, Oct. 1985.

[12]Yeh, H.Y., "Radiative Properties and Heat Transfer Analysis of Fibrous Insulations," Ph.D. Dissertation, The University of Mississippi, University, MS, in progress.

[13]Pantanker, S.V., *Numerical Heat Transfer and Fluid Flow*, Hemisphere Publishing Corp., Washington, DC, 1980.

[14]Chandrasekhar, S., *Radiative Transfer*, Dover Publications, Toronto, Canada, 1960.

[15]Hottel, H.C., Sarofim, A.F., Evans, L.B., and Vasalos, I.A., "Radiative Transfer in Anisotropically Scattering Media: Allowance for Fresnel Reflectance at the Boundaries," *Journal of Heat Transfer*, Vol. 90, Series C, Feb. 1968, pp. 56-62.

[16]Roux, J.A., Todd, D.C., and Smith, A.M., "Eigenvalues and Eigenvectors for Solutions to the Radiative Transport Equation," *AIAA Journal*, Vol. 10, July 1972, pp. 973-976.

[17]Roux, J.A. and Smith, A.M., "Radiative Transport Analysis for Plane Geometry with Isotropic Scattering and Arbitrary Temperature," *AIAA Journal*, Vol. 12, Sept. 1974, pp. 1273-1277.

[18]Roux, J.A., Smith, A.M., and Todd, D.C., "Radiative Transfer with Anisotropic Scattering and Arbitrary Temperature for Plane Geometry," *AIAA Journal*, Vol. 13, Sept. 1975, pp. 1203-1211.

[19]Viskanta, R., "Heat Transfer by Conduction and Radiation in Absorbing and Scattering Materials," *Journal of Heat Transfer*, Vol. 87, Series C, Feb., 1965, pp. 143-150.

[20]Schuetz, M.A., "Heat Transfer in Foam Insulation," Masters Thesis, MIT, Cambridge, MA, Dec. 1982.